DOA Estimation of Linear Dipole Arrays Based on Horse Herd Optimization Algorithm

Mohamed Bensalem and Ouarda Barkat

University of Freres Mentouri Constantine 1, Constantine, Algeria

https://doi.org/10.26636/jtit.2026.1.2422

Abstract — Subspace-based direction of arrival (DOA) estimation algorithms, such as MUSIC and ESPRIT, are designed for adaptive smart antenna arrays. However, these subspace methods require a large number of signal snapshots and sufficient angular separation between signals to provide an accurate DOA estimation of RF signal sources. Moreover, their resolution degrades significantly in severe noise scenarios. This study proposes a swarm intelligence (SI) algorithm, known as horse herd optimization (HOA), to address these limitations. An optimizer is employed as a direction-finding method to estimate the directions of arrival (DoAs) of incident signals impinging on a linear array of half-wavelength dipole (HWD) antennas by examining the global minimum of a non-linear cost function. This cost function is defined as the difference between the actual and estimated angles and is used to evaluate candidate solutions. Simulation results of the proposed algorithm have been compared with other recognized algorithms, including ESPRIT, root-MUSIC, and PSO, to verify estimation accuracy, convergence behavior, robustness against the number of elements, noise, and snapshots over Monte Carlo trials. It has been observed that the suggested HOA achieves better performance with a few snapshots, outperforms PSO and subspace-based methods when it comes to estimating DOA of incoming signals, particularly in a low signal-to-noise ratio (SNR) environment, and even when only fewer snapshots are available.

Keywords — DOA estimation, horse herd optimization, linear dipole arrays

1. Introduction

Over the past two decades, we have witnessed impressive growth in wireless communication systems. In light of this growth, advanced-generation wireless communication technologies, known as beyond 5G (B5G) or 6G networks, are emerging as powerful solutions to enhance system capacity, ensure reliable connectivity, and increase spectral efficiency [1], [2]. In such systems, smart dipole array antennas play a crucial role in supporting higher data rates and wider bandwidths, while enhancing system performance and capacity by increasing the gain in the desired direction of arrival (DOA) of the signal [3]–[5].

In general, a smart antenna system consists of an array of antenna elements arranged following a specific geometric pattern and equipped with a signal processor to accomplish two essential tasks: DOA estimation of all incoming signals and computation of optimal weights for adaptive beamforming [6], [7]. Before the beamforming process, the DOAs must be accurately estimated from the information received by the antenna array elements using an appropriate DOA estimation algorithm. The estimated directions then enable the beamforming technique to extract the signal of interest in the presence of interference and noise by forming a narrow beam toward the signal of interest (SOI) and placing nulls toward interfering signals, referred to as signals not of interest (SNOIs). Therefore, DOA estimation is a critical process in smart antenna systems, as it provides accurate directional information about signal sources in wireless communication networks [8], [9].

Estimation is a research domain in array signal processing, and DOA algorithms are an important part of this field. In general, these algorithms can be classified into two categories: those of deterministic and stochastic variety [10]. Although they differ in terms of accuracy, computational complexity, and convergence speed, several deterministic DOA estimation algorithms have been investigated in the literature for adaptive smart antenna arrays.

These algorithms can be mainly divided into three classes: conventional methods, subspace-based methods, and maximum likelihood techniques [11]. Owing to their simplicity and ability to accurately and efficiently resolve incoming signals, subspace-based DOA algorithms, such as multiple signal classification (MUSIC) and estimation of signal parameters via rotational invariance techniques (ESPRIT), have achieved significant success within the scientific community. These high-resolution algorithms share similar underlying principles [12]–[14]. They estimate the DOA by applying eigen-decomposition to the sample covariance matrix (SCM) of the received signals, exploiting orthogonality between the signal and noise subspaces. However, ESPRIT relies solely on the signal subspace.

Despite their advantages, these algorithms fail to provide accurate estimates in challenging scenarios, such as low signal-to-noise ratio (SNR) conditions and closely spaced sources [9], [15]. Moreover, they require a large number of signal snapshots to reliably estimate the SCM [9], which may not always be available in dynamic environments. Therefore, stochastic algorithms are employed to address these limitations.

Stochastic algorithms are predominantly metaheuristic methods. Techniques of this kind are generally flexible, provide reliable solutions, are easy to implement and are adaptable to a wide range of optimization problems [16], [17]. High-level metaheuristic search methods explore the search space randomly to avoid local optima and to identify the global optimum solution. They are typically inspired by natural behaviors observed in humans and animals, physical phenomena, evolutionary concepts, or other optimization paradigms [18], [19]. For this reason, they are referred to as nature-inspired metaheuristic algorithms and are commonly classified into four main categories according to their sources of inspiration: evolution-based, physics-based, swarm-based, and human-based algorithms [18], [20].

The swarm intelligence (SI) algorithms have gained significant popularity among researchers in recent years. These algorithms mimic the collective behavior of animals by employing multiple interacting agents that cooperate to solve optimization problems. The search process usually begins with a population of randomly generated candidate solutions which are subsequently refined through an iterative improvement process.

In the field of array signal processing (ASP), several SI algorithms have been proposed for DOA estimation, e.g. particle swarm optimization (PSO) [21], genetic algorithms (GA) [22], ant colony optimization (ACO) [23], bee colony optimization (BCO) [24], flower pollination algorithm (FPA) [25], squirrel search algorithm (SSA) [26], grey wolf optimization (GWO) [27], and chicken swarm optimization (CSO) [28].

SI algorithms typically begin with a population of randomly generated candidate solutions. Each algorithm employs a fitness function to evaluate the population, update candidate solutions, and search for the optimal solution using stochastic mechanisms.

According to the no free lunch (NFL) theorem [29], no single algorithm is capable of solving all optimization problems effectively, despite the wide diversity of existing metaheuristic approaches. Consequently, the primary challenge for these algorithms lies in achieving an appropriate balance between exploration and exploitation throughout the search process.

A recently proposed algorithm, known as the horse herd optimization algorithm (HOA), is inspired by the natural behaviors of horses belonging to different age groups [30]–[32]. This algorithm has demonstrated excellent performance in solving several real-world optimization problems. Owing to its effective exploration–exploitation strategy, HOA shows strong potential for addressing complex optimization problems across various application domains.

It is important to emphasize that the proposed approach strictly follows the conventional mathematical formulation of DOA estimation, while HOA is employed solely as a numerical global optimization tool to solve the resulting non-linear optimization problem. In this framework, each candidate solution represents a possible set of DOA estimates, and the optimization process aims at minimizing a signal-model-based cost function that quantifies the mismatch between the received signals and their reconstructed counterparts.

The novelty of this paper lies in the use of a HOA metaheuristic algorithm that is deployed as an estimator for determining the DOAs of multiple incident signals. Performance of the proposed algorithm is evaluated using simulation and measurements, with a particular emphasis placed on estimation accuracy, resolution capability, robustness to noise, robustness with respect to the number of snapshots through Monte Carlo simulations, and convergence speed.

Simulation results show that the proposed HOA-based estimator achieves excellent DOA estimation performance under extremely challenging conditions, including closely spaced sources, a limited number of snapshots, and severe noise, when applied to a linear array of HWD antennas. Moreover, the proposed method is compared with particle swarm optimization (PSO), root-MUSIC, and ESPRIT algorithms. The results demonstrate that the HOA-based approach outperforms these conventional methods in estimating the DOAs of incident signals impinging on a linear HWD antenna array.

In addition, a computational complexity analysis is provided to clarify the practical usefulness of the proposed method. Unlike subspace-based techniques, the proposed approach does not require the computation of the spatial covariance matrix nor spectral peak searching, which contributes to a reduced computational burden.

2. Problem Formulation

In a smart antenna system (SAS), DOA estimation refers to the process of extracting the directional information of multiple electromagnetic waves from the outputs of several receiving antennas using array signal processing techniques. These techniques exploit the fact that an electromagnetic wave impinging on an antenna array reaches each array element at different time instants.

In this work, an adaptive dipole array system is considered, which represents a type of smart antenna equipped with adaptive beamforming and DOA estimation capabilities, as illustrated in Fig. 1. The system consists of an array of half-wavelength dipole antennas, complex weighting coefficients, a summation unit, and a signal processing module [6], [9]. The smart antenna system employs a dipole array combined with advanced signal processing algorithms to estimate the DOAs of the incoming signals and subsequently compute the beamforming vectors, enabling electronic steering of the array output.

2.1. Objective Function

We consider L uncorrelated narrowband source signals impinging on an array of M antennas with different time delays. These sources generate plane waves, denoted by $s_l(t)$, arriving from distinct directions $\{\theta_1, \theta_2, \ldots, \theta_L\}$, and they also include additive zero-mean Gaussian noise (AWGN). For narrowband signals, the propagation time delays across the antenna elements can be equivalently represented as phase shifts.

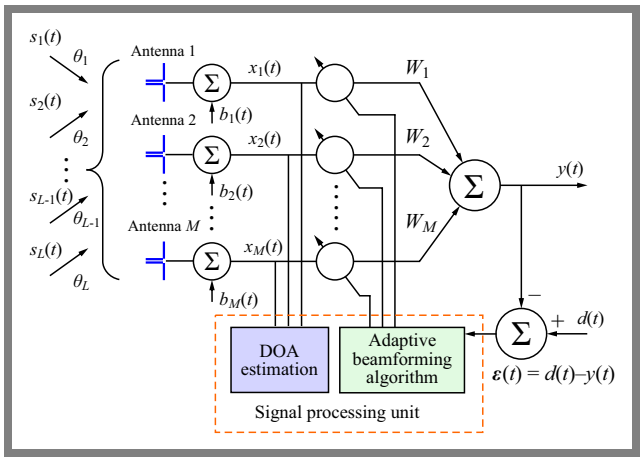

Fig. 1. Functional block diagram of an adaptive dipole array system.

Under ideal conditions, the steering vector is assumed to be perfectly known and depends solely on the array geometry and the directions of arrival. Consequently, the received signal vector of dimension $M \times 1$ can be written as:

$$x_m(t) = \sum_{i=1}^{L} e^{-j\frac{2\pi d(m-1)\sin(\theta_i)}{\lambda}} s_i(t) + b_m(t), \quad m = 1, 2, \ldots, M \,. \tag{1}$$

We can express Eq. (1) in matrix form as follows:

$$\mathbf{x}(t) = \mathbf{A}(\boldsymbol{\theta})\,\mathbf{s}(t) + \mathbf{b}(t)\,, \tag{2}$$

where $\bar{\mathbf{s}}(t)$ represents the original signals from the L sources with directions of arrival (DOAs) $\theta_1, \theta_2, \ldots, \theta_L$, and $\bar{\mathbf{b}}(t)$ denotes an additive noise vector whose components have zero-mean and variance σ^2.

The matrix $\bar{\mathbf{A}}(\boldsymbol{\theta})$ represents the steering vectors corresponding to the L sources for an array of M antennas, defined as:

$$\bar{\mathbf{x}}(t) = [\,x_1(t),\, x_2(t),\, \ldots,\, x_M(t)\,]^T\,, \tag{3}$$

$$\bar{\mathbf{b}}(t) = [\,b_1(t),\, b_2(t),\, \ldots,\, b_M(t)\,]^T\,, \tag{4}$$

$$\bar{\mathbf{s}}(t) = [\,s_1(t),\, s_2(t),\, \ldots,\, s_L(t)\,]^T\,, \tag{5}$$

$$\bar{\mathbf{A}}(\boldsymbol{\theta}) = [\,\bar{\mathbf{a}}(\theta_1),\, \bar{\mathbf{a}}(\theta_2),\, \ldots,\, \bar{\mathbf{a}}(\theta_L)\,]\,. \tag{6}$$

The steering vector $\bar{\mathbf{a}}(\theta_i)$ is given by:

$$\bar{\mathbf{a}}(\theta_i) = \left[1,\; e^{-j\frac{2\pi d\sin(\theta_i)}{\lambda}},\; \ldots,\; e^{-j\frac{2\pi d(M-1)\sin(\theta_i)}{\lambda}}\right]^T\,. \tag{7}$$

This study examines an array of M dipole elements, each half a wavelength long, spaced equally at a distance d. When an incoming wave carrying a baseband signal $s(t)$ impinges on the antenna array at an incident angle θ_i, the steering matrix $\bar{\mathbf{A}}(\boldsymbol{\theta})$ of the linear array corresponding to the source arriving from direction θ_i $(i = 1, \ldots, L)$ is given by:

$$\bar{\mathbf{A}}(\boldsymbol{\theta}) = \begin{bmatrix} 1 & \cdots & 1 \\ e^{-j\frac{2\pi d\sin(\theta_1)}{\lambda}} & \cdots & e^{-j\frac{2\pi d\sin(\theta_L)}{\lambda}} \\ \vdots & \ddots & \vdots \\ e^{-j\frac{2\pi d(M-1)\sin(\theta_1)}{\lambda}} & \cdots & e^{-j\frac{2\pi d(M-1)\sin(\theta_L)}{\lambda}} \end{bmatrix}_{M\times L}\,, \tag{8}$$

where the dimension of $\bar{\mathbf{A}}(\boldsymbol{\theta})$ is an $M \times L$ matrix, with each column corresponding to one of the M directional antennas.

The spatial covariance matrix $\mathbf{R}_{xx}$ of the observed signal vector $\bar{\mathbf{x}}(t)$, based on N signal samples at the array output, is given by:

$$\bar{\mathbf{R}}_{xx} = \mathbb{E}\left[\bar{\mathbf{x}}\,\bar{\mathbf{x}}^H\right] = \frac{1}{N}\sum_{i=1}^{N} \bar{\mathbf{x}}(i)\,\bar{\mathbf{x}}^H(i)\,, \tag{9}$$

where $(\cdot)^H$ denotes the Hermitian transpose operation.

By substituting Eq. (2) into Eq. (9), and assuming that $\bar{s}(t)$ and $\bar{b}(t)$ are uncorrelated and statistically independent, the covariance matrix can be written as:

$$\bar{\mathbf{R}}_{xx} = \bar{\mathbf{A}}(\boldsymbol{\theta})\,\bar{\mathbf{R}}_{ss}\,\bar{\mathbf{A}}^H(\boldsymbol{\theta}) + \sigma_b^2\,\mathbf{I}_M\,, \tag{10}$$

where $\mathbf{I}_M$ is the $M \times M$ identity matrix, and $\bar{\mathbf{R}}_{ss} = \mathbb{E}[\bar{\mathbf{s}}(t)\bar{\mathbf{s}}^H(t)]$ is the signal covariance matrix.

To solve any problem using the HOA algorithm, a fitness function has to be defined first, which will be used to evaluate the quality of possible solutions. For the purpose of DOA estimation, HOA can be employed to optimize the directions of arrival of the incident signals impinging on the antenna array by making the estimated angles approximately match the actual angles.

Accordingly, the following fitness function is applied for the evaluation, defined as:

$$f(\boldsymbol{\theta}) = \|\bar{\mathbf{x}}_a(t) - \bar{\mathbf{x}}_e(t,\boldsymbol{\theta})\|^2\,, \tag{11}$$

where $\bar{\mathbf{x}}_a(t)$ represents the actual received signal, which is expressed as:

$$\bar{\mathbf{x}}_a(t) = \bar{\mathbf{A}}(\boldsymbol{\theta}_a)\,\bar{\mathbf{s}}(t) + \bar{\mathbf{b}}(t)\,. \tag{12}$$

The estimated received signal, denoted by $\bar{\mathbf{x}}_e(t,\boldsymbol{\theta})$, can be expressed after obtaining the optimal solution as follows:

$$\bar{\mathbf{x}}_e(t,\boldsymbol{\theta}) = \bar{\mathbf{A}}(\boldsymbol{\theta})\,\hat{\mathbf{s}}(t)\,. \tag{13}$$

It should be noted that the vector $\bar{\mathbf{s}}(t)$ is unknown but common to both the actual and the estimated received signals. Its contribution is implicitly accounted for through the minimization of the fitness function $f(\boldsymbol{\theta})$. Accordingly, the SI-based estimator aims to determine the optimal DOA parameter vector $\boldsymbol{\theta}$ by searching for the values that minimize the objective function.

Therefore, the DOA estimation problem formulated in Eq. (11) can be rewritten as follows:

$$\min_{\boldsymbol{\theta}\in\mathcal{S}}\; f(\boldsymbol{\theta})\,, \tag{14}$$

where $\mathcal{S} \subset \mathbb{R}^L$ denotes the solution space.

The performance of each candidate solution is evaluated based on its corresponding fitness value. The initial population is randomly generated with a predefined population size. The HOA evaluation process is performed iteratively over T iterations using a population of N individuals until the stopping criterion is satisfied when the maximum number of iterations is reached $(t = T)$. Accordingly, the population at the t-th iteration can be represented as a collection of

L-dimensional vectors, given by:

$$\boldsymbol{\Theta}^{(t)} = \{\boldsymbol{\theta}_1^{(t)}, \boldsymbol{\theta}_2^{(t)}, \boldsymbol{\theta}_3^{(t)}, \ldots, \boldsymbol{\theta}_N^{(t)}\} . \tag{15}$$

The HOA-based approach is well suited for solving multidimensional optimization problems. Therefore, the position $\boldsymbol{\theta}^*$ corresponding to the minimum value of the fitness function $f(\boldsymbol{\theta})$ represents the estimated directions of arrival of the impinging signals. The DOA estimate at iteration t can thus be expressed as:

$$\boldsymbol{\theta}_{best}^{(t)} = \arg \min_{\boldsymbol{\theta}_i^{(t)} \in \{\boldsymbol{\theta}^{(t)}\}} f(\boldsymbol{\theta}_i^{(t)}) . \tag{16}$$

2.2. DOA Estimation with HOA

Horse herd optimization algorithm (HOA) is a modern swarm intelligence-based metaheuristic approach proposed in [30]. This algorithm is inspired by the behavioral patterns of horses in a herd, in their natural habitat, throughout their lifetime. During different stages of their lives, horses exhibit distinct behaviors that can be categorized into six primary groups: grazing (G), hierarchy (H), sociability (S), imitation (I), defense mechanism (D), and roaming (R). Their typical lifespan is approximately 25 – 30 years [33]. In this context, horses are labeled based on their age categories: δ represents horses between 0 and 5 years old, γ represents ages from 5 to 10, β represents ages ranging from 10 to 15, while α denotes horses that are over 15 years old. The emulation of the horses movement during each iteration is described in [30].

$$\mathbf{X}_n^{(\mathrm{iter},\mathrm{age})} = \mathbf{V}_n^{(\mathrm{iter},\mathrm{age})} + \mathbf{X}_n^{(\mathrm{iter}-1,\mathrm{age})}, \quad \mathrm{age} = \alpha, \beta, \gamma, \delta , \tag{17}$$

where $\mathbf{X}_n^{(\mathrm{iter},\mathrm{age})}$ indicates the position of the n-th horse, $\mathbf{V}_n^{(\mathrm{iter},\mathrm{age})}$ denotes the velocity vector of the considered horse during movement, while $\mathrm{iter}, \mathrm{age}$ represent the current iteration and the age category of each horse, respectively.

In each iteration, horses within the herd are organized, in the response matrix, from best to worst based on their fitness values. The selection process of horse ages in each iteration is guided by the rules of the HOA algorithm according to the following criteria [30]:

- α group horses are the most experienced and achieve the best response – they comprise the top 10% of the sorted population,
- β group horses follow, representing 20% of the total horse population,
- γ and δ group horses account for 30% and 40% of the remaining population, respectively.

Six distinct horse behaviors are specifically used to identify the velocity vector. Accordingly, the velocity vector of horses at different ages during every iteration of the algorithm is formulated as [30]:

$$\mathbf{V}_n^{(\mathrm{iter},\alpha)} = \mathbf{G}_n^{(\mathrm{iter},\alpha)} + \mathbf{D}_n^{(\mathrm{iter},\alpha)}, \tag{18}$$

$$\mathbf{V}_n^{(\mathrm{iter},\beta)} = \mathbf{G}_n^{(\mathrm{iter},\beta)} + \mathbf{H}_n^{(\mathrm{iter},\beta)} + \mathbf{S}_n^{(\mathrm{iter},\beta)} + \mathbf{D}_n^{(\mathrm{iter},\beta)}, \tag{19}$$

$$\begin{aligned}\mathbf{V}_n^{(\mathrm{iter},\gamma)} = \mathbf{G}_n^{(\mathrm{iter},\gamma)} + \mathbf{H}_n^{(\mathrm{iter},\gamma)} + \mathbf{S}_n^{(\mathrm{iter},\gamma)} \\ + \mathbf{I}_n^{(\mathrm{iter},\gamma)} + \mathbf{D}_n^{(\mathrm{iter},\gamma)} + \mathbf{R}_n^{(\mathrm{iter},\gamma)},\end{aligned} \tag{20}$$

$$\mathbf{V}_n^{(\mathrm{iter},\delta)} = \mathbf{G}_n^{(\mathrm{iter},\delta)} + \mathbf{I}_n^{(\mathrm{iter},\delta)} + \mathbf{R}_n^{(\mathrm{iter},\delta)} . \tag{21}$$

In the following, we describe the primary steps related to individual and social intelligence of horses, including the mathematical model for each behavior pattern.

2.3. Grazing

As herbivorous animals, horses primarily obtain their food from plants, grasses, and forages. The grazing behavior is exhibited by horses throughout their entire lives, at all age stages. As part of their daily routine, they spend most of their time grazing on pastures, devoting up to 16 – 20 h per day to this activity [33], and rest for only a very short period. The HOA optimizer emulates the grazing region around every horse by using a coefficient denoted as g, such that every horse grazes at specific locations. Equations (19) and (20) are employed to describe the grazing behavior of horses mathematically [30].

$$\begin{aligned}\mathbf{G}_n^{(\mathrm{iter},\mathrm{age})} = & g_n^{(\mathrm{iter},\mathrm{age})} \left(\hat{\mathbf{u}} + \hat{\mathbf{P}}_l\right) \times \mathbf{X}_n^{(\mathrm{iter}-1,\mathrm{age})}, \\ & \mathrm{age} = \alpha, \beta, \gamma, \delta ,\end{aligned} \tag{22}$$

$$g_n^{(\mathrm{iter},\mathrm{age})} = g_n^{(\mathrm{iter}-1,\mathrm{age})} \times \omega_g . \tag{23}$$

Here $\mathbf{G}_n^{(\mathrm{iter},\mathrm{age})}$ refers to the parameter of describing grazing movement of the horse, which reflects the horse's proclivity to graze. This parameter decreases linearly with a reduction coefficient ω_g per iteration.

P is a randomly generated number between $[0, 1]$, while $\hat{\mathbf{l}}$ and $\hat{\mathbf{u}}$ denote the lower and upper boundaries of the grazing area, respectively, as recommended in [30], and are set to 0.95 and 1.05. Also, the coefficient g is set to 1.5 at the start of the search process for all age ranges.

2.4. Hierarchy

The second behavior of horses considered by the HOA algorithm is *hierarchy*. Horses are social animals and typically live under the guidance of a leader, similar to certain human social structures. In the wild, the herd is led by the dominant leader, who is the most experienced and strongest horse, often a mature stallion or mare, responsible for supervising and guiding the herd. In the HOA algorithm, the parameter h illustrates the proclivity of horses to pursue the most experienced and strongest horse. Studies have shown that horses in the middle age groups, β and γ, adhere to the hierarchy rule. The mathematical expressions describing this behavior are as follows [30]:

$$\begin{aligned}\mathbf{H}_n^{(\mathrm{iter},\mathrm{age})} = & h_n^{(\mathrm{iter},\mathrm{age})} \times \left(\mathbf{X}_*^{(\mathrm{iter}-1)} - \mathbf{X}_n^{(\mathrm{iter}-1)}\right) \\ & \mathrm{age} = \alpha, \beta, \gamma ,\end{aligned} \tag{24}$$

$$h_n^{(\mathrm{iter},\mathrm{age})} = h_n^{(\mathrm{iter}-1,\mathrm{age})} \times \omega_h . \tag{25}$$

Here, $\mathbf{H}_n^{(\text{iter,age})}$ signifies the level of the horse's hierarchy, indicating how the best horse's location impacts the velocity parameter. $\mathbf{X}_*^{(\text{iter}-1)}$ denotes the position of the best horse in the previous iteration. At the start of the search process, the parameter h is initialized to 1.5, 0.9, and 0.5 for horses of ages α, β, and γ, respectively, while ω_h represents the hierarchy reduction coefficient [30].

2.5. Sociability

Horses typically exhibit social behavior, allowing them to coexist with other livestock, including cattle and sheep, and they often enjoy their company rather than being solitary in their natural environment. Since the hunting habits of predators threaten the safety of wild horses, herd life significantly enhances their security, reduces their likelihood of predation, and facilitates escape from predators.

Horses may occasionally engage in disputes and can display irritability due to their individuality. Notably, the *sociability* behavior is most commonly observed in horses aged between 5 and 15 years. In the HOA algorithm, this behavior is modeled as the tendency of a horse to move toward the average position of other horses, as expressed in the following mathematical formulas [30]:

$$\mathbf{S}_n^{(\text{iter,age})} = s_n^{(\text{iter,age})} \left[\frac{1}{N} \sum_{j=1}^{N} \mathbf{X}_j^{(\text{iter}-1)} - \mathbf{X}_n^{(\text{iter}-1)} \right], \quad \text{age} \in \{\beta, \gamma\}, \tag{26}$$

$$s_n^{(\text{iter,age})} = s_n^{(\text{iter}-1,\text{age})}\, \omega_s . \tag{27}$$

In Eqs. (26) and (27), $\mathbf{S}_n^{(\text{iter,age})}$ represents the social movement vector of the n-th horse, while $s_n^{(\text{iter,age})}$ denotes the horse's tendency to move toward the herd during the i-th iteration. The parameter $s_n^{(\text{iter,age})}$ is reduced in each iteration by a sociability reduction coefficient, ω_s. Here, N represents the total number of horses.

2.6. Imitation

The social nature of horses within a herd allows them to share and learn both positive and negative behaviors by imitating one another [34], such as identifying suitable grazing locations. Juvenile horses have the propensity to mimic the more senior ones, and such an instinct pattern lasts until they reach adulthood. This behavior is commonly observed in horses up to 10 years old (i.e., γ horses). In the HOA algorithm, the parameter i represents the imitation behavior of horses, as described below [30]:

$$\mathbf{I}_n^{(\text{iter,age})} = i_n^{(\text{iter,age})} \left[\frac{1}{pN} \sum_{j=1}^{pN} \hat{\mathbf{X}}_j^{(\text{iter}-1)} - \mathbf{X}_n^{(\text{iter}-1)} \right], \quad \text{age} = \gamma , \tag{28}$$

$$i_n^{(\text{iter,age})} = i_n^{(\text{iter}-1,\text{age})} \times \omega_i . \tag{29}$$

where $\mathbf{I}_n^{(\text{iter, age})}$ denotes the imitation movement vector of the n-th horse toward the average position of the best horses with estimated locations $\hat{\mathbf{X}}$, and ω_i represents the imitation reduction coefficient. Moreover, pN denotes the number of horses with the best positions, where p is typically set to 10% of the herd size. It is also suggested that ω_i be set to 0.3 for age γ [30].

2.7. Defense Mechanism

Another behavioral aspect of horses considered in the HOA algorithm is *defense*. Horses' defensive reactions reflect their natural status as prey animals. Instinctively, horses compete for water and nourishment to eliminate rivals and avoid dangerous areas and predators. When confronted with a threatening situation, horses exhibit a *fight-or-flight* response to protect themselves, with fleeing being their primary reaction. They may also buck violently and neigh loudly when caught in a trap.

In the HOA optimizer, the horses' defense mechanism is modeled such that a horse moves away from other horses with inferior positions that are far from the optimal solution. This defensive behavior is maintained throughout the entire lifespan of both young and adult horses. Equations (30) and (31) describe the defense mechanism of horses using a negative parameter d, which forces the current horse to stay away from unsuitable locations [30].

$$\vec{D}_n^{(\text{iter,age})} = -d_n^{(\text{iter,age})} \left(\frac{1}{qN} \sum_{j=1}^{qN} \check{\mathbf{X}}_j^{(\text{iter}-1)} - \mathbf{X}_n^{(\text{iter}-1)} \right), \quad \text{age} \in \{\alpha, \beta, \gamma\}, \tag{30}$$

$$d_n^{(\text{iter,age})} = d_n^{(\text{iter}-1,\text{age})}\, \omega_d , \tag{31}$$

where $\vec{D}_n^{(\text{iter, age})}$ represents the escape vector of the n-th horse from those with the worst locations, which are indicated by the vector $\check{\mathbf{X}}$. The term qN denotes the number of horses occupying the worst positions in the current population, with a recommended value of $0.2N$ according to [30]. The parameter ω_d represents the defense reduction coefficient at each iteration. It is also suggested that the initial value of the parameter d for α, β, and γ be set to 0.5, 0.2, and 0.1, respectively, at the beginning of the search process [30].

2.8. Roam

The final behavioral pattern incorporated in the HOA algorithm is *roaming*. Horses naturally graze and move from one pasture to another in search of nourishment. Although the majority of horses are retained in stables, they preserve an innate tendency to roam. A horse may unexpectedly change its grazing location. Their curious nature drives them to explore new grasslands and learn their positions. To accommodate this curiosity, the side walls of stables are designed to allow horses to see one another [30]. A stochastic movement is more pronounced in young horses and gradually decreases as they reach full maturity. The HOA algorithm models this behavior as a random movement characterized by a parameter r. This process is expressed as follows [30]:

$$\vec{R}_n^{(\text{iter,age})} = r_n^{(\text{iter,age})}\, \mathbf{P}\mathbf{X}_n^{(\text{iter}-1,\text{age})}, \quad \text{age} = \gamma, \delta \tag{32}$$

$$r_n^{(\mathrm{iter,age})} = r_n^{(\mathrm{iter}-1,\mathrm{age})}\ \omega_r\ . \tag{33}$$

In the above equations, $\vec{R}_n^{(\mathrm{iter,age})}$ represents the random velocity vector of the n-th horse used for local search and to escape from local minima. The parameter ω_r denotes the imitation reduction coefficient for $r_n^{(\mathrm{iter,age})}$ at each iteration. For ages γ and δ, it is recommended to set the initial values of r to 0.05 and 0.1, respectively [30]. By substituting Eqs. (23) – (33) into Eqs. (19) – (22), the velocity vector for each age group can be obtained.

Velocity of δ horses at the age of 0 – 5 years:

$$\begin{aligned}\vec{V}_m^{(\mathrm{iter},\delta)} = &\left[g_m^{(\mathrm{iter}-1,\delta)}\ \omega_g\ (\hat{\mathbf{u}} + \hat{\mathbf{P}}_l)\ \mathbf{X}_m^{(\mathrm{iter}-1)}\right] \\ &+ \left[i_m^{(\mathrm{iter}-1,\delta)}\ \omega_i\ \Big(\frac{1}{pN}\sum_{j=1}^{pN}\hat{\mathbf{X}}_j^{(\mathrm{iter}-1)} - \mathbf{X}_m^{(\mathrm{iter}-1)}\Big)\right] \\ &+ \left[r_m^{(\mathrm{iter}-1,\delta)}\ \omega_r\ \mathbf{P}\mathbf{X}_m^{(\mathrm{iter}-1)}\right]\ .\end{aligned} \tag{34}$$

Velocity of γ horses at the age of 5 – 10 years:

$$\begin{aligned}\vec{V}_m^{(\mathrm{iter},\gamma)} = &\left[g_m^{(\mathrm{iter}-1,\gamma)}\ \omega_g\ (\hat{\mathbf{u}} + \hat{\mathbf{P}}_l)\ \mathbf{X}_m^{(\mathrm{iter}-1)}\right] \\ &+ \left[h_n^{(\mathrm{iter}-1,\gamma)}\ \omega_h\ (\mathbf{X}_*^{(\mathrm{iter}-1)} - \mathbf{X}_n^{(\mathrm{iter}-1)})\right] \\ &+ \left[s_n^{(\mathrm{iter}-1,\gamma)}\ \omega_s\ \Big(\frac{1}{N}\sum_{j=1}^{N}\mathbf{X}_j^{(\mathrm{iter}-1)} - \mathbf{X}_n^{(\mathrm{iter}-1)}\Big)\right] \\ &+ \left[i_n^{(\mathrm{iter}-1,\gamma)}\ \omega_i\ \Big(\frac{1}{pN}\sum_{j=1}^{pN}\hat{\mathbf{X}}_j^{(\mathrm{iter}-1)} - \mathbf{X}_n^{(\mathrm{iter}-1)}\Big)\right] \\ &- \left[d_n^{(\mathrm{iter}-1,\gamma)}\ \omega_d\ \Big(\frac{1}{qN}\sum_{j=1}^{qN}\check{\mathbf{X}}_j^{(\mathrm{iter}-1)} - \mathbf{X}_n^{(\mathrm{iter}-1)}\Big)\right] \\ &+ \left[r_n^{(\mathrm{iter}-1,\gamma)}\ \omega_r\ \mathbf{P}\mathbf{X}_n^{(\mathrm{iter}-1)}\right]\ .\end{aligned} \tag{35}$$

Velocity of β horses at the age of 10 – 15 years:

$$\begin{aligned}\vec{V}_n^{(\mathrm{iter},\beta)} = &\left[g_n^{(\mathrm{iter}-1,\beta)}\ \omega_g\ (\hat{\mathbf{u}} + \hat{\mathbf{P}}_l)\ \mathbf{X}_n^{(\mathrm{iter}-1)}\right] \\ &+ \left[h_n^{(\mathrm{iter}-1,\beta)}\ \omega_h\ (\mathbf{X}_*^{(\mathrm{iter}-1)} - \mathbf{X}_n^{(\mathrm{iter}-1)})\right] \\ &+ \left[s_n^{(\mathrm{iter}-1,\beta)}\ \omega_s\ \Big(\frac{1}{N}\sum_{j=1}^{N}\mathbf{X}_j^{(\mathrm{iter}-1)} - \mathbf{X}_n^{(\mathrm{iter}-1)}\Big)\right] \\ &- \left[d_n^{(\mathrm{iter}-1,\beta)}\ \omega_d\ \Big(\frac{1}{qN}\sum_{j=1}^{qN}\check{\mathbf{X}}_j^{(\mathrm{iter}-1)} - \mathbf{X}_n^{(\mathrm{iter}-1)}\Big)\right]\ .\end{aligned} \tag{36}$$

Velocity of α horses older than 15 years:

$$\begin{aligned}\vec{V}_n^{(\mathrm{iter},\alpha)} = &\ g_n^{(\mathrm{iter}-1,\alpha)}\ \omega_g\ (\hat{\mathbf{u}} + \hat{\mathbf{P}}_l)\ \mathbf{X}_n^{(\mathrm{iter}-1)} \\ &- d_n^{(\mathrm{iter}-1,\alpha)}\ \omega_d\ \left(\frac{1}{qN}\sum_{j=1}^{qN}\check{\mathbf{X}}_j^{(\mathrm{iter}-1)} - \mathbf{X}_n^{(\mathrm{iter}-1)}\right)\ .\end{aligned} \tag{37}$$

The pseudo-code and the flowchart of the HOA algorithm are illustrated as Algorithm 1 and in Fig. 2.

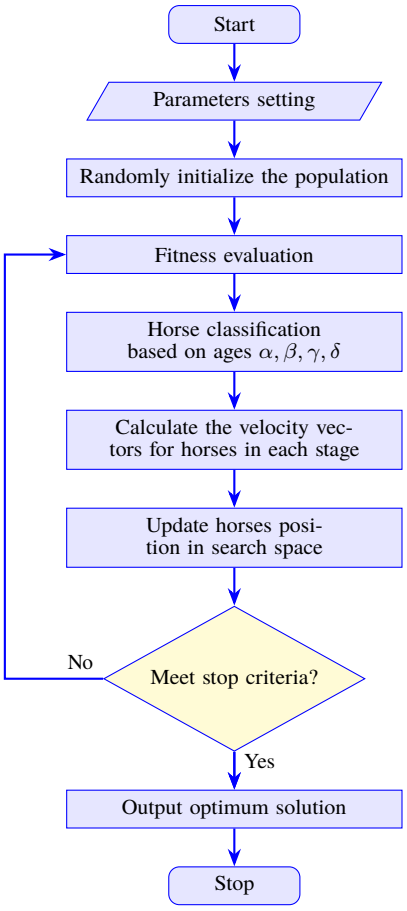

Fig. 2. Flowchart of the HOA algorithm.

3. Numerical Results and Discussions

A comprehensive comparative analysis is performed against root-MUSIC, ESPRIT, and PSO algorithms to validate the effectiveness of the proposed optimizer. This study includes four major evaluation criteria: estimation accuracy, convergence behavior, robustness against the number of elements, noise, and snapshots, and RMSE performance based on Monte Carlo simulations.

To perform these simulations, a uniform linear array (ULA) of isotropic point sources consisting of $M = 8$ half-wavelength dipoles is considered, with an inter-element spacing of half a wavelength. This spacing is selected to mitigate mutual coupling effects between adjacent dipoles. In all scenarios, the narrowband sources impinging on the ULA from different directions are assumed to be uncorrelated, and the added noise is Gaussian white noise. The simulations are carried out using 20 snapshots and 2400 Monte Carlo trials. For DOA estimation using the HOA algorithm, the fitness values are evaluated by searching for the global minimum of a non-linear cost function corresponding to the adopted ULA array, as defined in Eq. (11).

The HOA and PSO algorithms are implemented in Matlab with a maximum of 100 iterations. The search space for the uniform linear array is defined over the angular range of 0 to $180°$. For the HOA algorithm, the number of horses is set

to $N = 50$, and the control parameters h^{β}, h^{γ}, s^{β}, s^{γ}, i^{γ}, d^{α}, d^{β}, d^{γ}, r^{δ}, and r^{γ} are assigned values of 0.9, 0.5, 0.2, 0.1, 0.3, 0.5, 0.2, 0.1, 0.1, and 0.05, respectively. For the PSO algorithm, the swarm size is set to 200 particles, the cognitive and social acceleration coefficients are fixed at $C_1 = C_2 = 2$, and the inertia weight is linearly varied between $W_1 = 0.9$ and $W_2 = 0.4$.

In the first simulation, histograms of the DOA estimates obtained using the HOA optimizer are presented for $L = 3$ sources with DOAs at $[30°, 60°, 120°]$, and for $L = 4$ sources with DOAs at $[30°, 50°, 70°, 90°]$, as illustrated in illustrated in Fig. 3. These histograms represent the probability of a signal arriving from a given direction. Averaging the histograms over consecutive data blocks improves both the accuracy and reliability of the analysis. The peaks of the resulting angular probability distributions provide estimates of the DOAs.

Algorithm 1 Pseudo code of the horse herd optimization algorithm

Start

1: Define input parameters specific to the problem, including their corresponding constraints and algorithm parameters
2: Set $Itr = 1$
3: Initialization: Generate initial horse positions randomly and uniformly distributed throughout the search space between θ_{min} and θ_{max}
4: Fitness evaluation: Evaluate the fitness of each horse's position according to the objective function described in Eq. (11)
5: **while** $Itr \leqslant Itr_{max}$ **do**
6: **for** $i = 1$ to total number of horses **do**
7: Sort the locations of horses in ascending order based on their fitness values
8: Organize the horses into α, β, γ, and δ classes according to their age ranges
9: Compute the velocity vectors for horses in each class using Eqs. (22) to (25)
10: Update the positions of all horses by applying the corresponding movement vectors according to Eq. (21).
11: **end for**
12: Fitness evaluation: Evaluate the fitness of each horse's updated position using the objective function in Eq. (11).
13: Update best solution:
14: **if** new fitness value < the previous best fitness value **then**
15: • Set the new position as the best position
16: • Set the new fitness value as the best fitness value
17: **end if**
18: $Itr = Itr + 1$
19: **end while**
20: Return the best solution

End

The results indicate that the proposed algorithm yields highly accurate joint DOA estimates, with distinct peaks occurring precisely at the true angles. Moreover, estimation accuracy of the HOA algorithm is comparable to that reported in [12]. However, unlike subspace-based methods which require a large number of snapshots to construct the covariance matrix (CM), the proposed approach achieves accurate DOA estimation with a significantly smaller number of snapshots.

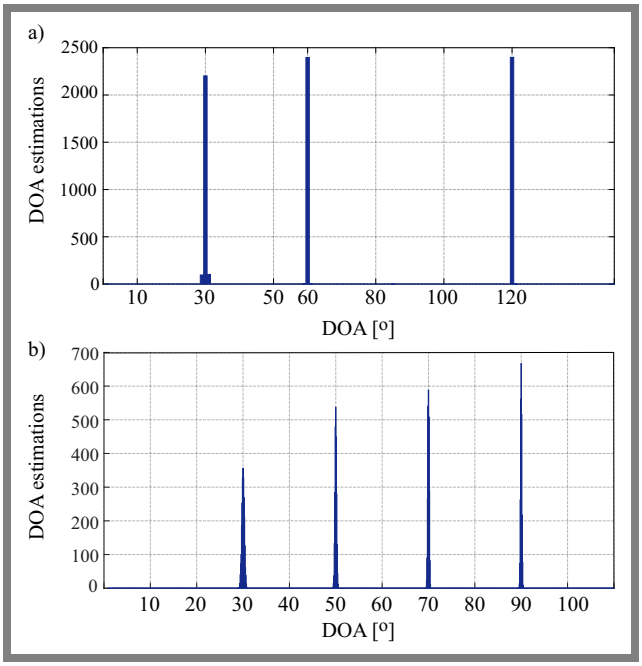

Fig. 3. Histogram of DOA estimations for HOA algorithm: a) $L = 3$ sources located at [30°, 60°, 120°] with $SNR = [5, 5, 5]$ dB, inter-element spacing $d = \lambda/2$, and an array of $M = 8$ elements, and b) $L = 4$ sources located at [30°, 50°, 70°, 90°] with $SNR = [5, 5, 5, 5]$ dB.

In the second simulation experiment, a statistical analysis is performed for the HOA, PSO, root-MUSIC, and ESPRIT algorithms to evaluate their ability to precisely and efficiently resolve incoming signals. The performance assessment is based on several statistical metrics, including the best, worst, mean, standard deviation (STD), and variance, which enhance the reliability of the experimental results.

This analysis examines the DOA estimation accuracy of the considered algorithms under three different scenarios: two sources with directions $L = [60°, 65°]$, three sources with directions $L = [60°, 70°, 80°]$, and four sources with directions $L = [60°, 70°, 80°, 90°]$, all at an SNR of -5 dB. The corresponding histograms are illustrated in Figs. 4, 5, while the statistical results obtained from 2400 Monte Carlo trials are summarized in Tabs. 1 – 3.

From Fig. 4a, it is evident that distinct peaks appear around 60°and 65°without any estimation failure when using the HOA algorithm. In contrast, the PSO algorithm successfully estimates the two DOAs, as indicated by the presence of two clear peaks around 60° and 65° in Fig. 4b. However, an undesired spurious peak appears at 115°, suggesting that PSO converges to a suboptimal solution during the DOA estimation process.

Furthermore, no dominant peaks corresponding to the true directions of arrival are observed in Figs. 4c-d. Instead, the estimated angles are widely dispersed over the range of 0 to 180°, indicating that the ESPRIT and root-MUSIC algorithms fail to provide reliable DOA estimates under this scenario.

The statistical results reported in Tab. 1 further confirm the superiority of the proposed approach. The HOA algorithm consistently yields more accurate DOA estimates across mul-

Tab. 1. Statistical results obtained from the comparative algorithms with two signal sources.

Angle	Algorithm	Best [°]	Average [°]	Worst [°]	STD [°]	Variance
60°	HOA	60.0003218	60.0084690	62.0928421	0.50195	0.251962
	PSO	60.0002743	59.9963548	63.5189249	0.87261	0.761442
	ESPRIT	60.0030129	55.1508742	1.1694029	11.8465	140.3399
	root-MUSIC	60.0228375	55.1782856	1.2533743	14.0110	196.3082
65°	HOA	64.9993400	64.9979923	63.4006353	0.46555	0.216737
	PSO	65.0006115	85.7792229	118.1794532	24.6773	608.9697
	ESPRIT	64.9922174	82.5666223	179.1887797	26.8622	721.5804
	root-MUSIC	65.0031988	100.3000588	179.5411878	31.1882	972.7084

Tab. 2. Statistical results obtained from the comparative algorithms with three signal sources.

Angle	Algorithm	Best [°]	Average [°]	Worst [°]	STD [°]	Variance
70°	HOA	70.0003199	70.0027179	71.9030490	0.483988	0.234245
	PSO	69.9997522	70.0841697	74.8310570	1.330736	1.770858
	ESPRIT	69.9993590	66.9298423	139.974860	11.81534	139.60224
	root-MUSIC	69.9980060	60.7203797	1.2675782	17.10490	292.57776
80°	HOA	80.0004090	79.9888340	81.8906260	0.472660	0.223407
	PSO	79.9985383	80.9648580	102.110770	4.156118	17.27331
	ESPRIT	80.0003768	80.7862460	157.564900	8.075658	65.21624
	root-MUSIC	80.0205634	82.0559765	131.482520	7.951755	63.23040
90°	HOA	90.0002380	90.0080280	92.1217950	0.439226	0.192919
	PSO	89.9999996	90.3872096	103.745127	4.528096	20.50365
	ESPRIT	90.0013500	95.1284890	176.143860	14.40636	207.54317
	root-MUSIC	89.9975326	110.933836	179.261060	24.60050	605.18449

Tab. 3. Statistical results obtained from the comparative algorithms with four signal sources.

Angle	Algorithm	Best [°]	Average [°]	Worst [°]	STD [°]	Variance
60°	HOA	59.999858	60.015577	58.064286	0.521405	0.271863
	PSO	60.000583	60.001719	57.074942	0.855451	0.731797
	ESPRIT	60.017033	55.614013	0.346814	11.88656	141.2903
	root MUSIC	60.000541	50.870238	0.665556	16.57344	274.6788
70°	HOA	69.999971	69.999257	68.186362	0.484881	0.235110
	PSO	69.999927	70.054767	75.944602	1.299854	1.689620
	ESPRIT	69.998388	70.449175	45.331282	6.557652	43.00281
	root MUSIC	70.011308	71.892475	95.026589	8.179528	66.90468
80°	HOA	79.999460	80.003784	81.610049	0.454403	0.206482
	PSO	79.999663	80.793881	101.15362	4.088790	16.71820
	ESPRIT	80.004837	82.124547	105.91682	6.549457	42.89539
	root MUSIC	79.987492	87.897832	132.00127	10.37003	107.5375
90°	HOA	90.000030	90.106479	154.89177	2.632250	6.928739
	PSO	90.000004	90.550814	103.67308	4.535886	20.57426
	ESPRIT	89.996200	101.91026	179.00447	20.29290	411.8016
	root MUSIC	90.000406	121.50774	178.77402	23.78936	565.9337

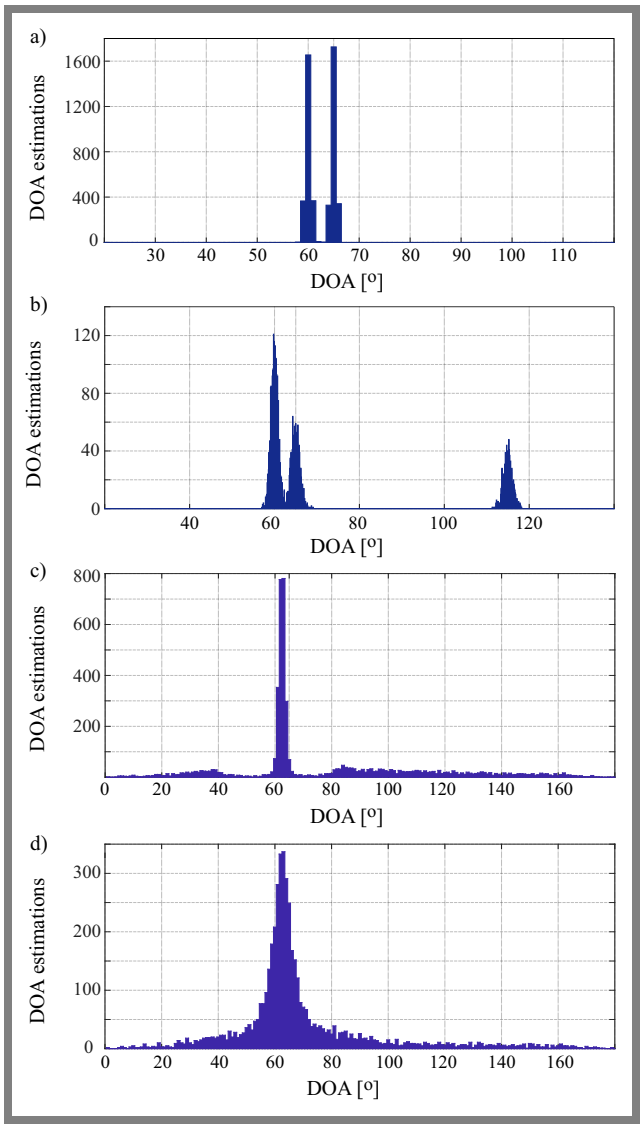

Fig. 4. Histogram of DOA estimations for $L = 2$ sources located at [60°, 65°], with SNR = [–5, –5] dB, inter-element spacing $d = \lambda/2$, and an array of $M = 8$ elements, using: a) HOA, b) PSO, c) root-MUSIC, and d) ESPRIT.

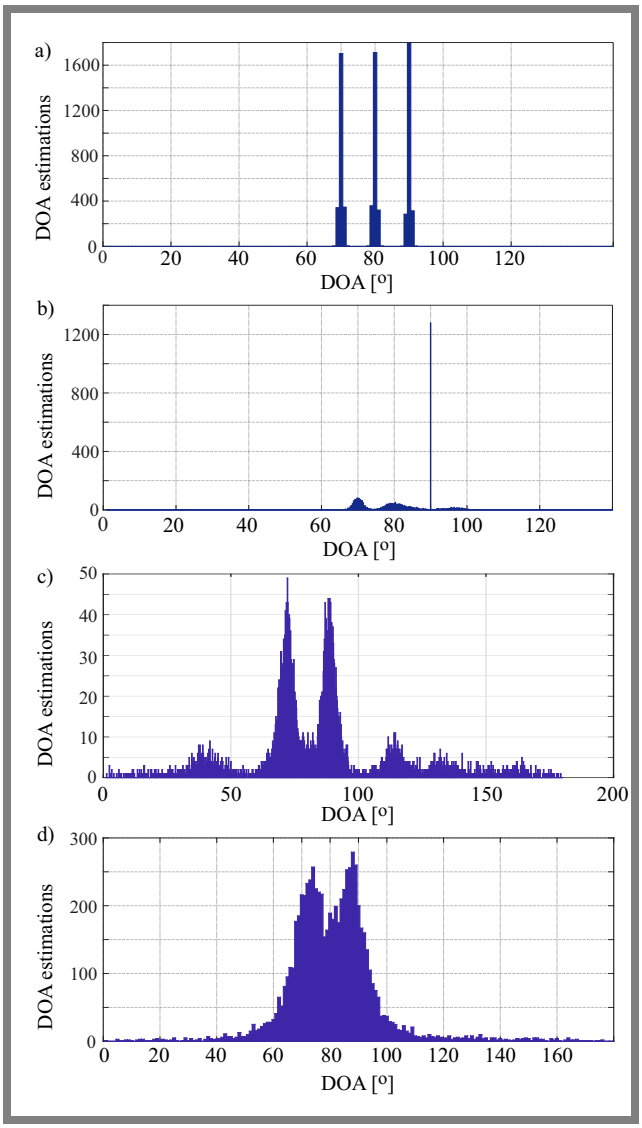

Fig. 5. Histogram of DOA estimations for $L = 3$ sources located at [70°, 80°, 90°], with SNR = [–5, –5, –5] dB, inter-element spacing $d = \lambda/2$, and an array of $M = 8$ elements, using: a) HOA, b) PSO, c) root-MUSIC, and d) ESPRIT algorithms.

tiple independent Monte Carlo simulations, achieving the best performance in terms of best, average, and worst estimated angles, while also exhibiting the smallest variance and standard deviation relative to PSO, ESPRIT and root-MUSIC.

Figure 5a illustrates that the proposed SI-based algorithm provides the most accurate DOA estimations with high resolution, where three distinct and well-defined peaks are clearly observed around 70°, 80°, and 90°. In comparison, the PSO algorithm is able to estimate the three DOAs, as shown in Fig. 5b. However, an undesired spurious peak appears at an unintended angle, indicating suboptimal convergence.

On the other hand, the root-MUSIC algorithm does not consistently yield accurate DOA estimates, for scattered estimates are observed around the true DOA peaks, as illustrated in Fig. 5c. Moreover, the ESPRIT algorithm completely fails to provide reliable DOA estimations in this scenario, since no dominant peaks are observed near the actual angles and the estimated directions are widely dispersed, as shown in Fig. 5d.

Table 3 summarizes the performance comparison among PSO, root-MUSIC, and ESPRIT for this scenario. Once again, the HOA algorithm demonstrates significantly better performance by achieving the most accurate DOA estimates, with best, average, and worst estimated angles closely matching the true directions. Furthermore, it exhibits the lowest variance and standard deviation.

Figure 6a shows that the proposed algorithm achieves highly accurate joint DOA estimation by producing sharp histograms for the corresponding DOA estimates. As can be clearly observed, the exact peaks occur at [60°, 70°, 80°, 90°] without any estimation failure. In contrast, the results obtained using the PSO algorithm, shown in Fig. 6b, are inferior to those of the HOA algorithm, as an additional spurious peak appears around 97°, indicating suboptimal estimation performance.

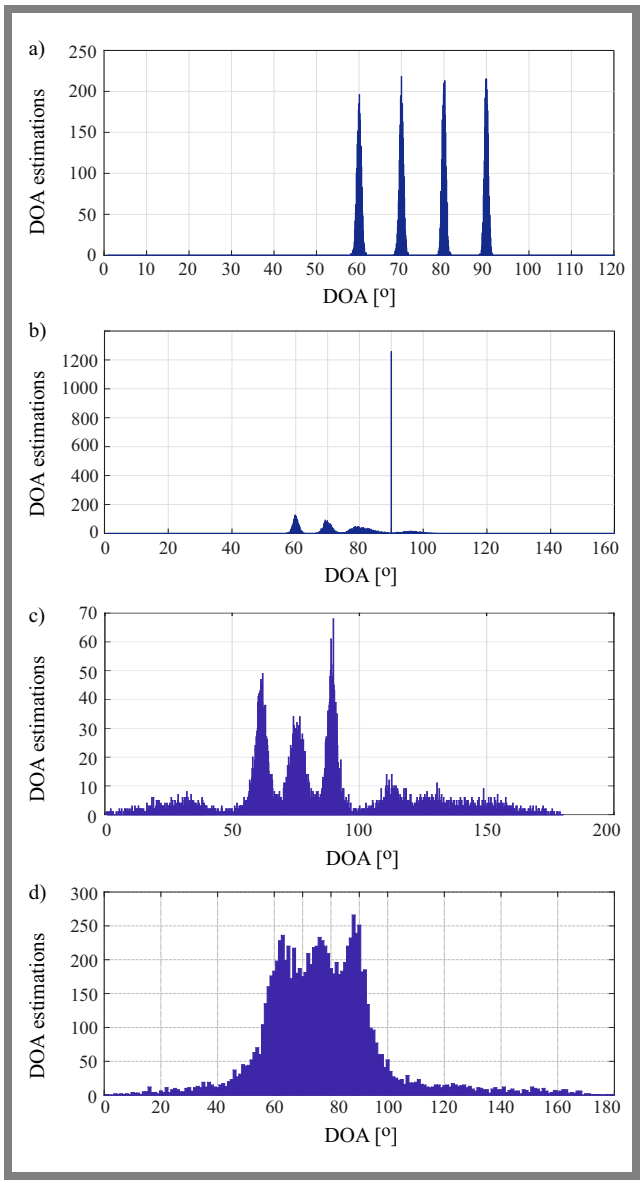

Fig. 6. Histogram of DOA estimates for $L = 4$ sources located at [60°, 70°, 80°, 90°], with SNRs of [–5,–5,–5, –5] dB, inter-element spacing $d = \lambda/2$, and $M = 8$ antenna elements, using: a) HOA, b) PSO, c) root-MUSIC, and d) ESPRIT algorithms.

Furthermore, as shown in Figs. 6c-d, no clear peaks are observed around the true angles of arrival, revealing that the DOA estimation performance of the ESPRIT and root-MUSIC algorithms is very poor and suffers from large estimation errors.

The statistical results presented in Tab. 4 further confirm the superiority of the HOA algorithm.

Tab. 4. Computational complexity analysis.

Algorithm	Computational complexity
HOA / PSO	$O(M \cdot K \cdot L \cdot \text{Iter} \cdot N)$
ESPRIT	$O(M^3 + M^2K)$
MUSIC	$O(M^3 + M^2K + M^2Q)$
root-MUSIC	$O(M^3 + M^2K)$

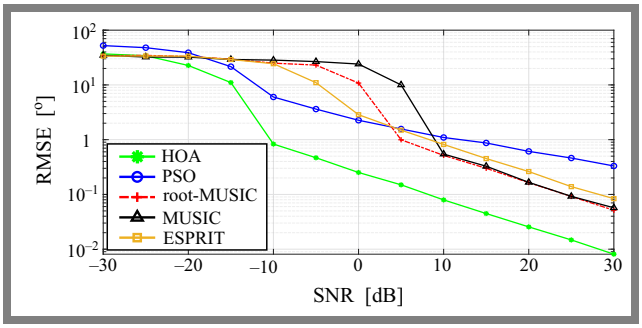

Fig. 7. Root mean square error versus SNR for DOA.

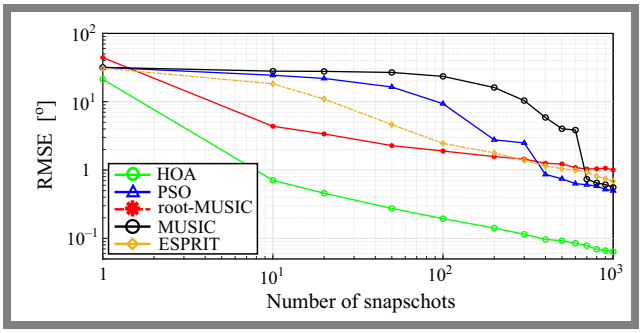

Fig. 8. Root mean square error versus snapshots for DOA.

In the third simulation, we evaluate the performance of the proposed algorithm using the root mean square error (RMSE) as the performance metric, which quantifies how close the estimated angles are to the true angles of the signal sources. The RMSE is calculated using the following equation:

$$\text{RMSE} = \sqrt{\frac{1}{VL}\sum_{v=1}^{V}\sum_{l=1}^{L}(\hat{\theta}_{l,v} - \theta_l)^2}\,, \tag{38}$$

where $\theta_{l,v}$ denotes the estimated DOA of the l-th source, and V represents the number of Monte Carlo trials, set to 200, used to average the performance.

The evaluation is conducted by varying the signal-to-noise ratio (SNR), the number of snapshots, and the number of array elements.

In the first case, the effect of SNR on the performance of the algorithms is evaluated. Figure 7 illustrates the RMSE curves of the algorithms under different SNR conditions. We consider a scenario where the SNR varies in the range of [–30, 30] dB, with 20 snapshots and $M = 8$ antenna elements.

According to the RMSE values, the error rates of the different algorithms are very high when SNR is –30 dB. As the SNR increases, the RMSE of all algorithms gradually decreases, leading to more accurate DOA estimates. Moreover, the proposed algorithm consistently exhibits lower RMSE than the PSO, root-MUSIC, and ESPRIT algorithms under the same noise conditions. Specifically, under low SNR conditions (SNR < 0 dB), the proposed algorithm outperforms all other algorithms, demonstrating excellent robustness against noise.

In the second case, the impact of the number of snapshots on the performance of each algorithm is examined. Plots of the RMSE as a function of the number of snapshots for all algorithms are illustrated in Fig. 8, where the number of

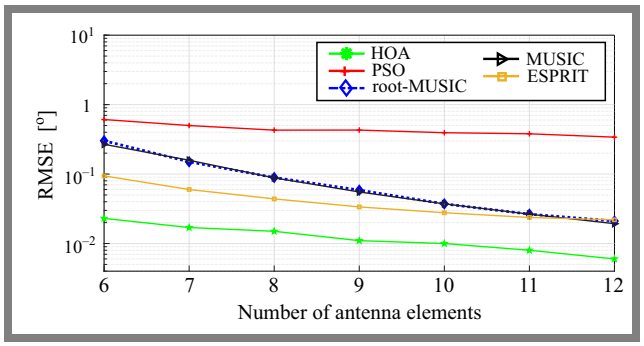

Fig. 9. Root mean square error versus number of antenna elements for DOA.

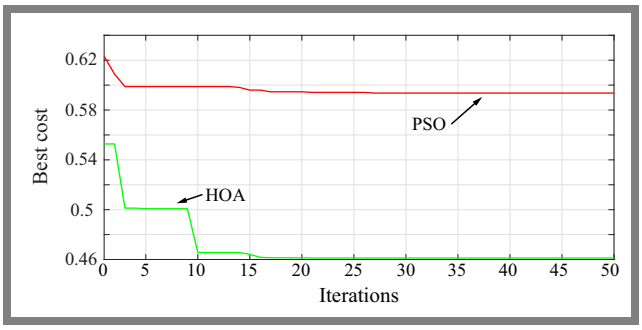

Fig. 10. Convergence characteristics of the fitness value versus the number of iterations.

snapshots varies in the range of [20, 1000], with $M = 8$ and SNR = –5 dB.

The results indicate that the accuracy of DOA estimation using the HOA, PSO, root-MUSIC, MUSIC, and ESPRIT algorithms is heavily influenced by the number of snapshots. Under conditions with few snapshots, the error rate of the subspace algorithms is very high, demonstrating a significant deterioration in estimation resolution. In contrast, the proposed HOA algorithm consistently demonstrates greater robustness when fewer snapshots are available for DOA estimation, with its error reduced to zero above just 20 snapshots. This makes the method particularly well-suited for situations with limited data. As the number of snapshots increases (beyond 10 snapshots), RMSE gradually decreases, indicating improved estimation accuracy. This improvement is expected because subspace methods require a large number of stationary time samples to capture the statistical properties necessary for accurately estimating the covariance matrix.

In this third scenario, we evaluate and compare the estimation accuracy of all previously mentioned methods by monitoring RMSE against the number of antenna elements. This scenario considers seven different values for antenna elements ($M = 6, 7, 8, 9, 10, 11, 12$) at SNR of 25 dB, using 20 snapshots. The relationship between RMSE and the number of antenna elements M is depicted in Fig. 9. It is evident that as the number of antenna elements M incresase, the error decreases, exhibiting substantial improvement in estimation accuracy for all techniques. Furthermore, the HOA and CSA algorithms provide better estimation resolution, outperforming the PSO, ESPRIT, and root-MUSIC methods across the simulated range of antenna elements.

Finally, the process of finding the optimal solution using the proposed algorithm is illustrated through convergence graphs which track the progression of the best solution at each iteration. Figure 10 presents the normalized average fitness values against the number of generations for the HOA and PSO algorithms. The figure shows that the proposed HOA algorithm converges faster than the PSO algorithm and can typically obtain near-optimal solutions more quickly when estimating the angles of incoming signals.

Table 4 provides a comparative summary of computational complexity, including subspace-based algorithms (ESPRIT, MUSIC, and root-MUSIC), PSO, and the proposed HOA approach. The main contributors to the computational complexity of the subspace-based algorithms are covariance matrix estimation, eigenvalue decomposition, and angular spectrum scanning.

However, ESPRIT and root-MUSIC avoid the spectral peak searching required by MUSIC. Therefore, the parameters associated with these algorithms are the number of array elements M, the number of signal snapshots K, the number of sources L, and the number of scanning angles Q. The complexity of ESPRIT primarily comes from the covariance estimation $O(M^2K)$ and the eigen-decomposition process $O(M^3)$, resulting in an overall complexity of $O(M^3 + M^2K)$. On the other hand, the computational complexity of the MUSIC algorithm mainly stems from covariance matrix estimation $O(M^2K)$, eigenvalue decomposition $O(M^3)$, and angular spectrum scanning $O(M^2Q)$, giving a total complexity of $O(M^3 + M^2K + M^2Q)$. Root-MUSIC avoids spectral peak searching by converting the MUSIC spectrum into a polynomial rooting problem. Its computational complexity is dominated by covariance estimation and polynomial rooting, resulting in $O(M^3 + M^2K)$. Consequently, MUSIC has higher computational complexity due to its peak-searching approach in the spatial pseudo-spectrum.

In contrast, swarm intelligence (SI) algorithms such as PSO and HOA avoid matrix eigen-decomposition and spectral peak searching. These approaches are primarily governed by the number of times the cost function is evaluated and the size of the operations in each evaluation.

In each iteration of the SI-based algorithm, a set of candidate solutions is generated. Evaluating each candidate requires constructing a steering matrix based on the estimated angles, estimating the source signals, and calculating the received signal reconstruction error. These operations involve matrix operations whose complexity is proportional to M and K. Consequently, the overall complexity increases linearly with the number of antenna elements M, snapshots K, and sources L, and also depends on the number of iterations and population size, resulting in $O(M \cdot K \cdot L \cdot \mathrm{Iter} \cdot N)$

Although the HOA-based approach incurs higher complexity than the subspace algorithms, the overall complexity remains polynomial and can be adjusted by selecting the population size and the number of iterations. This offers a favorable trade-off between estimation accuracy and computational cost, particularly in multi-source and low-SNR scenarios. According to the literature, a qualitative comparison among

the maximum likelihood (ML) algorithm [35], subspace-based methods, swarm-intelligence-based approaches, and the proposed HOA algorithm can be summarized as follows.

The ML algorithm achieves very high accuracy under ideal conditions but suffers from low robustness in noisy environments and has very high computational complexity. Subspace-based methods, such as MUSIC, root-MUSIC, and ESPRIT, provide high accuracy under favorable conditions. However, their performance degrades at low SNR and with a limited number of snapshots due to their reliance on covariance matrix estimation.

Swarm-intelligence-based approaches, such as PSO, offer moderate accuracy and robustness but remain computationally demanding because of their iterative optimization process. In contrast, the proposed HOA algorithm demonstrates high accuracy with strong robustness in low-SNR and limited-snapshot scenarios while maintaining moderate computational complexity, thus providing a favorable trade-off between performance and computational cost.

4. Conclusions

The performance of most DOA estimation algorithms, such as MUSIC and ESPRIT, deteriorates significantly in challenging scenarios, such as high noise levels or when sources are closely spaced. Moreover, these algorithms require a large number of snapshots to maintain the accuracy of the estimated DOAs of incident signals.

In this paper, we propose a DOA estimation method to address these challenges. Through extensive simulations, the proposed method is compared with several well-known algorithms, including ESPRIT, root-MUSIC, and PSO. Simulation results show that HOA achieves the highest resolution, particularly at low SNRs and for small angular separations between sources. Additionally, experimental results confirm the robustness and effectiveness of the HOA algorithm. They also prove that is consistently outperforms these methods in terms of RMSE across various scenarios, including different SNR levels, numbers of snapshots, and numbers of array elements.

Overall, the main advantage of the proposed HOA-based DOA estimation lies in its ability to accurately detect signal angles with a limited number of snapshots, making it particularly suitable for real-time implementation when data collection is constrained.

References

[1] N. Ruan, H. Wang, F. Wen, and J. Shi, "DOA Estimation in B5G/6G: Trends and Challenges", *Sensors*, vol. 22, art. no. 5125, 2022 (https://doi.org/10.3390/s22145125).

[2] A.E. Zorkun, M.A. Salas-Natera, R.M. Rodrıguez-Osorio, and S. Chatzinotas, "Energy Efficient Low-complexity RIS-aided 3-D DoA Estimation and Target Tracking Algorithm via Matrix Completion", *IEEE Access*, vol. 12, pp. 197929–197941, 2024 (https://doi.org/10.1109/ACCESS.2024.3511717).

[3] V. Dakulagi and M. Bakhar, "Smart Antenna System for DOA Estimation Using Single Snapshot", *Wireless Personal Communications*, vol. 107, pp. 81–93, 2019 (https://doi.org/10.1007/s11277-019-06241-0).

[4] O. Barkat, "Capon DOD/DOA Estimation Algorithm for Bistatic MIMO Radar Using Dipole Antenna Arrays with Known Mutual Coupling", *Journal of Telecommunications and Information Technology*, vol. 101, pp. 1–7, 2025 (https://doi.org/10.26636/jtit.2025.3.2121).

[5] S.K. Imtiaj, I.S. Misra, and S. Bhattacharya, "Revisiting Smart Antenna Array Design with Multiple Interferers Using Basic Adaptive Beamforming Algorithms: Comparative Performance Study with Testbed Results", *Engineering Reports*, vol. 3, pp. 1–32, 2020 (https://doi.org/10.1002/eng2.12295).

[6] F. Gross, *Smart Antenna for Wireless Communication*, New York: McGraw-Hill, 288 p., 2005 (ISBN: 9780071447898).

[7] N. Boughaba and O. Barkat, "LMS and RLS Beamforming Algorithms Based Linear Antenna Array with Known Mutual Coupling", *Journal of Electromagnetic Waves and Applications*, vol. 37, pp. 1449–1462, 2024 (https://doi.org/10.1080/09205071.2023.2251979).

[8] A. Kuchar *et al.*, "A Robust DOA-Based Smart Antenna Processor for GSM Base Stations", *IEEE International Conference on Communications*, Vancouver, Canada, 1999 (https://doi.org/10.1109/ICC.1999.767867).

[9] M. Bensalem and O. Barkat, "DOA Estimation of Linear Dipole Array with Known Mutual Coupling Based on ESPRIT and MUSIC", *Radio Science*, vol. 57, pp. 1–15, 2022 (https://doi.org/10.1029/2021RS007294).

[10] K. Hameed *et al.*, "DOA Estimation in Low SNR Environment through Coprime Antenna Arrays: An Innovative Approach by Applying Flower Pollination Algorithm", *Applied Sciences*, vol. 11, art. no. 7985, 2021 (https://doi.org/10.3390/app11177985).

[11] T.S. Bird, *Mutual Coupling Between Antennas*, UK: Wiley, 480 p., 2021 (ISBN: 9781119564980).

[12] K. Gowri and P. Palanisamy, "Two Dimensional Direction of Arrival Estimation Algorithm for Coherent Signals Using Three Parallel Uniform Linear Arrays", *Journal of Communications Technology and Electronics*, vol. 64, pp. 1383–1390, 2019 (https://doi.org/10.1134/S106422691912009X).

[13] R. Roy and T. Kailath, "ESPRIT–Estimation of Signal Parameters via Rotational Invariance Techniques", *IEEE Transactions on Acoustics, Speech, & Signal Processing*, vol. 37, pp. 984–995, 1989 (https://doi.org/10.1109/29.32276).

[14] R. Schmidt, "Multiple Emitter Location and Signal Parameter Estimation", *IEEE Transactions on Antennas and Propagation*, vol. 34, pp. 276–280, 1986 (https://doi.org/10.1109/TAP.1986.1143830).

[15] J. Yao *et al.*, "Satellite Interference Source Direction of Arrival (DOA) Estimation Based on Frequency Domain Covariance Matrix Reconstruction", *Sensors*, vol. 23, art. no. 7575, 2023 (https://doi.org/10.3390/s23177575).

[16] E. Talbi, *Metaheuristics from Design to Implementation*, John Wiley & Sons, 624 p., 2009 (ISBN: 978-0470278581).

[17] B. Morales-Castaneda *et al.*, "A Better Balance in Metaheuristic Algorithms: Does It Exist?", *Swarm and Evolutionary Computation*, vol. 54, art. no. 100671, 2020 (https://doi.org/10.1016/j.swevo.2020.100671).

[18] S. Mirjalili and A. Lewis, "The Whale Optimization Algorithm", *Advances in Engineering Software*, vol. 95, pp. 51–67, 2016 (https://doi.org/10.1016/j.advengsoft.2016.01.008).

[19] F. Fausto *et al.*, "From Ants to Whales: Metaheuristics for All Tastes", *Artificial Intelligence Review*, vol. 53, pp. 753–810, 2020 (https://doi.org/10.1007/s10462-018-09676-2).

[20] R. Rajakumar, P. Dhavachelvan, and T. Vengattaraman, "A Survey on Nature Inspired Meta-heuristic Algorithms with its Domain Specifications", *International Conference on Communication and Electronics Systems (ICCES)*, Coimbatore, India, 2016 (https://doi.org/10.1109/CESYS.2016.7889811).

[21] J.C. Chang, "DOA Estimation for Local Scattered CDMA Signals by Particle Swarm Optimization", *Sensors*, vol. 12, pp. 3228–3242, 2012 (https://doi.org/10.3390/s120303228).

[22] N. Ahmed *et al.*, "Performance Analysis of Efficient Computing Techniques for Direction of Arrival Estimation of Underwater Multi Targets", *IEEE Access*, vol. 9, pp. 33284–33298, 2021 (https://doi.org/10.1109/ACCESS.2021.3060819).

[23] W. Shi, J. Huang, and Y. Hou, "Fast DOA Estimation Algorithm for MIMO Sonar Based on Ant Colony Optimization", *Journal of Systems Engineering and Electronics*, vol. 23, pp. 173–178, 2012 (https://doi.org/10.1109/JSEE.2012.00022).

[24] S.A.H. Parsa, A.E. Zadeh, and S.J. Kazemitabar, "A Novel Modified Artificial Bee Colony for DOA Estimation", *International Journal of Sensors Wireless Communications and Control*, vol. 11, pp. 96–106, 2021 (https://doi.org/10.2174/2210327909666191209154508).

[25] S. Akbar *et al.*, "Flower Pollination Heuristics for Parameter Estimation of Electromagnetic Plane Waves", *Computer Modeling in Engineering & Sciences*, vol. 68, pp. 2529–2543, 2021 (https://doi.org/10.32604/cmc.2021.016097).

[26] M. Jain, V. Singh, and A. Rani, "A Novel Nature-inspired Algorithm for Optimization: Squirrel Search Algorithm", *Swarm and Evolutionary Computation*, vol. 44, pp. 148–175, 2019 (https://doi.org/10.1016/j.swevo.2018.02.013).

[27] N. Ahmed, H. Wang, M.A.Z. Raja, and W. Ali, "Novel Design of Grey Wolf Optimization Heuristics for High Resolution Direction of Arrival Estimation in Acoustic Plane Waves", *Wireless Personal Communications*, vol. 128, pp. 2507–2529, 2022 (https://doi.org/10.1007/s11277-022-10057-w).

[28] A. Sharma *et al.*, "Maximum Likelihood Direction of Arrival Estimation Using Chicken Swarm Optimization Algorithm", *International Journal of Mathematical Engineering and Management Sciences*, vol. 6, pp. 621–635, 2021 (https://doi.org/10.33889/IJMEMS.2021.6.2.038).

[29] D.H. Wolpert and W.G. Macready, "No Free Lunch Theorems for Optimization", *IEEE Transactions on Evolutionary Computation*, vol. 1, pp. 67–82, 1997 (https://doi.org/10.1109/4235.585893).

[30] F. MiarNaeimi, G. Azizyan, and M. Rashki, "Horse Herd Optimization Algorithm: A Nature-inspired Algorithm for High-dimensional Optimization Problems", *Knowledge-Based Systems*, vol. 213, art. no. 106711, 2021 (https://doi.org/10.1016/j.knosys.2020.106711).

[31] D.A. Elmanakhly, M. Saleh, E.A. Rashed, and M. Abdel-Basset, "BinHOA: Efficient Binary Horse Herd Optimization Method for Feature Selection: Analysis and Validations", *IEEE Access*, vol. 10, pp. 26795–26816, 2022 (https://doi.org/10.1109/ACCESS.2022.3156593).

[32] A. Refaat *et al.*, "Extraction of Maximum Power from PV System Based on Horse Herd Optimization MPPT Technique under Various Weather Conditions", *Renewable Energy*, vol. 220, art. no. 119718, 2024 (https://doi.org/10.1016/j.renene.2023.119718).

[33] K. Krueger and J. Heinze, "Horse Sense: Social Status of Horses (Equus Caballus) Affects Their Likelihood of Copying Other Horses' Behavior", *Animal Cognition*, vol. 11, pp. 431–439, 2008 (https://doi.org/10.1007/s10071-007-0133-0).

[34] F. Bogner, "A Comprehensive Summary of the Scientific Literature on Horse Assisted Education in Germany", Bachelor Thesis, Van Hall Larenstein University, 2011.

[35] P. Stoica and A. Nehorai, "MUSIC, Maximum Likelihood, and Cramer-Rao Bound", *IEEE Transactions on Acoustics, Speech, and Signal Processing*, vol. 37, pp. 720–741, 1989 (https://doi.org/10.1109/29.17564).

Mohamed Bensalem, M.Sc.
Electronic Department
https://orcid.org/
E-mail: mbensalem481@yahoo.fr
University of Freres Mentouri Constantine 1, Constantine, Algeria
http://www.umc.edu.dz

Ouarda Barkat, Professor
Electronic Department
https://orcid.org/0000-0001-6784-8338
E-mail: barkat.ouarda@umc.edu.dz
University of Freres Mentouri Constantine 1, Constantine, Algeria
http://www.umc.edu.dz